Trends in Photochemistry & Photobiology
Vol. 21, 2022

Original Article

Effect of dipeptide derivative Schiff-base Zn(II) complexes on lysozyme molecules damaged by means of IR-FEL irradiation

Yuika Onami[1], Takayasu Kawasaki[2], Tomoyuki Haraguchi[1], Koichi Tsukiyama[1,2], Dohyun Moon[3], Yasutaka Kitahama[4], Takuya Hosokai[4], Hiroyuki Matsuzaki[4], Hiroshi Sakiyama[5] and Takashiro Akitsu[1,*]

[1]Department of Chemistry, Faculty of Science, Tokyo University of Science, 1-3 Kagurazaka, Shinju-ku-ku, Tokyo 162-8601, Japan; [2]FEL-TUS, Tokyo University of Science, 2641 Yamazaki, Noda, Chiba 278-8510, Japan. [3]Pohang Accelerator Laboratory, Pohang University of Science and Technology (POSTECH), San-31 Hyoja-dong, Pohang, 790-784, Republic of Korea. [4]National Institute of Advanced Industrial Science and Technology, Tsukuba, Japan; [5]Department of Science, Faculty of Science, Yamagata University, 1-4-12 Kojirakawa, Yamagata 990-8560, Japan.

ABSTRACT

An infrared free-electron laser can decompose aggregated proteins (including metal complexes) *via* the excitation of their vibrational bands. In this study, using the results of previous studies on human serum albumin, we prepared hybrid materials of chicken egg white lysozyme protein with the same Schiff-base Zn(II) complexes by incorporating glycylglycine dipeptide derivative moieties. The analysis of secondary structures after irradiation indicated that the inclusion of the Zn(II) complexes into lysozyme induced structural changes in lysozyme, resulting in a more fragile structure than that of the original lysozyme; this is the second reported example of the enhancing effect of a metal complex on protein molecules damaged by IR-FEL irradiation. Their docking features *via* weak intermolecular interactions were also investigated using fluorescence spectra (quenching, temperature dependence, and decay lifetime) with the aid of computational simulation of docking.

KEYWORDS: lysozyme, dipeptide derivative, Schiff base, Zn(II) complex, infrared free-electron laser, luminescence.

*Corresponding author: akitsu2@rs.tus.ac.jp

1. INTRODUCTION

Free-electron lasers (FELs) are being applied in various fields of science [1-3]. Infrared free-electron laser (IR-FEL) irradiation applies to every phase—solid, liquid, and gas—that exhibits infrared absorption [4-9]. To date, it has been used in various fields, such as surgical treatment and gas-phase chemistry. Moreover, IR-FEL is expected to change the structure of various biologically related materials. Thus far, numerous studies have been conducted on the deformation of biomolecules by IR-FEL, although knowledge in this field has steadily accumulated only recently. The first step in modifying a molecular structure involves the instantaneous supply of adequate vibrational excitation energy to the chemical bond. Hence, the development of a novel method that involves IR-FEL irradiation to control the structure of biological materials is required. Herein, available reports of basic and applied research on IR-FEL related to biomolecules are reviewed. Thus far, IR-FEL has been useful in the biochemical and biological fields for treating skin and neurological diseases, materials science, and basic physical chemistry. For example, the amide I and II bands of myoglobin exhibit non-uniform temperature dependence. The long-wavelength side of the

amide band is composed of hydrogen atoms of amino acids. However, using a temperature-dependent band it was confirmed that vibrational energy flowed into the hydration shell [4].

The conformation of protonated glutamic acid (protonated glutamate separated by a quadrupole ion trap) was identified by vibrational spectroscopy and density functional theory (DFT) calculations at room temperature (about 300 K) and very low temperatures. Using an IR free-electron laser, the two most stable, almost-equal energy conformations were identified by the analysis of the infrared multiphoton dissociation spectrum recorded in the fingerprint range [5].

IR spectroscopy of ions accompanied by resonant IR multiphoton dissociation has been applied for the identification of novel psychotropic drugs (NPSs). The exact identification of the isomer of an NPS is forensically important because legal control depends on small molecular differences such as the position of a single ring substituent. Furthermore, research has shown that a closely related NPS can be distinguished with the assistance of computationally predicted IR spectra [6].

Laser surgical resection can help remove a limited amount of target tissue. In a previous study, optical imaging was used to assess lethal and sublethal collateral damage after FEL resection surgery. Results indicated that a wavelength of 6.10 μm is suitable for the laser ablation of the skin [7].

Permanent laser hair removal also benefits the selective photothermal degradation of sebaceous glands, a part of hair follicles. Sebaceous glands have been studied *in-vitro* using FEL pulses resonant with the vibrational absorption band of methylene [8]. A study that combined computation with IR multiphoton dissociation spectroscopy determined the folded structure of protonated *D*-(+)-biotin generated in the gas phase by electrospray ionization. The proton bonding between ureido and valeryl carbonyls was unambiguously identified, and only a single conformer of such a structure predominated [9].

The functions and structural changes of protein molecules are induced in special situations. Herein, we focus on proteins containing amyloid and metal ions. Misfolded protein aggregation and the progressive polymerization of soluble proteins are observed in various diseases, including muscle atrophic lateral sclerosis, cerebral amyloid angiopathy, type II diabetes, Parkinson's disease, Huntington's disease, and Alzheimer's disease. These are common features of highly debilitating and increasingly prevalent diseases [10]. Alzheimer's disease is the most common of the misfolding ("amyloid") disorders of proteins. Patient brain deposits contain an aggregated insoluble form of the amyloid β peptide. Interactional aggregation pathways between the amyloid β peptide and Cu(II) and Zn(II) ions and modifying small molecules have been reported [8]. The binding of a Cu(II) ion to the amyloid β peptide of amyloid fibrils increases Cu(II) ion levels in Alzheimer's amyloid plaques, and this binding of amyloid β to Cu(II) ions produces neurotoxic active oxygen species. The details of the investigation of the Cu(II) molecule that binds to amyloid fibrils have been reported [9]. Moreover, Cu(II) is an essential metal for normal human development and function, especially for the central nervous system [11]. However, its redox activity requires an accurate Cu(II) transport system [12]. The disease caused by mutations in ATP7A is the Cu(II) deficiency syndrome, which is promptly treated with Cu(II)-histidine injections after definitive diagnosis [13]. Numerous metalloproteases have also been reported to play critical roles in the development of various pathological conditions. Diseases wherein unnatural protein conformations cause protein aggregation are concerning [14].

To the best of our knowledge, the effect of IR-FEL irradiation on amyloid fibers has been reported in very few papers, mainly by Kawasaki *et al*. [15-17]. Fibrotic peptides such as amyloid fibrils are responsible for severe amyloidosis in humans. Fibril structures are typically difficult to dissociate due to their tightly stacked conformations. Previous research showed that the number of β-sheets decreased and those of other components, such as α-helices and turns, increased relative to that of fibrils before FEL irradiation [15]. The structure of amyloid β fibrils is tightly stacked in a β-sheet conformation, and the fibrillar state of amyloid β is closely related to the pathogenesis of Alzheimer's disease. The total content of proteins exhibiting a β-sheet structure decreased in the brain sections of the model mice. Mid-IR light dissociates the β-sheet

structure of amyloid β fibrils and is expected to be applied in laser-based therapies [16]. The aggregation of lysozyme in acidic solutions produces inactive amyloid-like fibrils. A previous study reported that the spontaneous refolding of these fibrils in water may be promoted by mid-IR-FEL irradiation targeting the amide band in β-sheet-rich structures [17].

In this context, we found that metal complexes promoted protein degradation. In previous studies target molecules such as proteins (human serum albumin (HSA)) [18, 19], Interleukin-6 (IL-6) [20], Schiff-base Zn(II) complex-containing proteins [18, 19], and amino acids [20], were irradiated by IR-FEL at appropriate wavelengths corresponding to amide I and II and imine C=N bands. Before and after irradiation, secondary structure analysis suggested that including two types of Schiff-base Zn(II) complexes in HSA rendered protein molecules fragile for damage by IR-FEL. According to the docking simulation of ligands into HSA proteins (PDB:1BM0A), the decomposition features suggest that weakly binding ligands may be attributed to structural changes in proteins. When the complex of these amino acid/dipeptide analogs and proteins is irradiated with IR-FEL, it can selectively cleave chemical bonds by the multiphoton absorption of IR. However, a closer examination indicated that the protein was easily damaged due to the disorder of the protein structure caused by the metal complex ligand.

To confirm the above considerations, herein, we will examine other proteins (egg white lysozyme (Lyz)), including identical Schiff-base Zn(II) complexes (ZnGlyGlyH and ZnGlyGlyPh) incorporating glycylglycine derivative ligands [19]. As reported previously [21], metal complexes have been designed to contain peptide bonds in a ligand (containing a dipeptide moiety and not an amino acid), and chemically stable and diamagnetic Zn(II) ions enable detection by fluorescence spectroscopy without the risk of reaction of metal centers. In contrast to previous studies on different Zn(II) complexes for the same protein (HSA), our present work aimed to compare different proteins (HSA and Lyz) using the same Zn(II) complexes (ZnGlyGlyH and ZnGlyGlyPh). The resulting conformational changes in the protein and the abundance of α-helices and β-sheets in the secondary structure before and after IR-FEL irradiation were determined using protein secondary structure analysis. Furthermore, several types of PL and other measurements were employed to investigate the effect and behavior of the weakly binding ligands of ZnGlyGlyH and ZnGlyGlyPh.

2. MATERIALS AND METHODS

2.1. Materials

Chicken egg white lysozyme and phosphate-buffered saline (PBS; 10 mM, pH 7.2–7.4 at 298 K) were procured from FUJIFILM Wako Pure Chemical Corporation (Osaka, Japan). Two Zn(II) complexes were prepared according to a previously reported procedure and used as identical samples [19].

2.2. Physical measurements

IR spectra were recorded in the transmission mode using KBr pellets for the Zn(II) complexes only and in the reflection mode as cast films for Lyz (and Zn complexes) using a stainless plate with a JASCO FT-IR 4200 plus spectrophotometer in the range of 400–4000 cm^{-1} at 298 K. Electronic (UV-vis) spectra were obtained using a JASCO V-570 UV-vis-NIR spectrophotometer in the range of 200–1500 nm at 298 K. Fluorescence spectra were obtained using a JASCO FP-6200 spectrophotometer in the range of 220–720 nm. Time-correlated single-photon counting (TCSPC) measurements were conducted using a FluoroCube (Horiba) at 298 K. For the excitation light source, a pulsed light-emitting diode (Horiba, NanoLED; wavelength of 342 nm, pulse width of 1 ns, and repetition rate of 1 MHz) was used. Fluorescence intensity was measured at 470 nm. Powder X-ray diffraction (PXRD) patterns were obtained with a Rigaku Smart Lab using a Cu Kα source or Pohang Light Source II 2D Supramolecular Crystallography Beamline (PLSII-2D-SMC); thereafter, they were processed using Rigaku (Tokyo, Japan) PDXL2 software, which produced preliminary results that were only used as starting models for DFT optimization.

2.3. Computational methods

The docking simulation of the ligand (models were constructed from the preliminary powder crystal structure of Zn(II) complexes, and their reasonable conformation was confirmed with computation)–

protein (PDB:5LYT crystal structure [22]) was conducted using the GOLD program (CCDC, UK) [23]. The models of Zn complexes used for docking computations were constructed using DFT calculations, performed using the GAMESS program [24, 25] on Fujitsu PRIMERGY CX2550/ CX2560 M4 (ITO supercomputer system) at Kyushu University. Structural optimization was conducted using an LC-BOP/6-31G* basis [26]. The solvent effect was simulated using the polarizable continuum model (PCM) method assuming two conditions, namely (i) in vacant and (ii) in water solvent.

2.4. IR-FEL Irradiation

Samples of ZnGlyGlyH and ZnGlyGlyPh as KBr pellets, cast films of an Lyz membrane, and Lyz and Lyz+ZnGlyGlyH or Lyz+ZnGlyGlyPh composite membranes were prepared for IR measurements. The formation of composites was confirmed by the spectral changes in the fluorescence and UV-vis spectra while maintaining predominantly secondary structures in the case of HSA [19]. IR-FEL was used at the Infrared-Free Electron Laser Research Center of the Tokyo University of Science (FEL-TUS) [27, 28]. According to a previously reported procedure [19], we empirically determined three representative wavelengths for IR-FEL irradiation: C=N double-bond band 6.12 μm (1634 cm^{-1}), amide I band 6.07 μm (1647 cm^{-1}), and amide II band 6.48 μm (1544 cm^{-1}). The intensity of the IR-FEL beam condenses was appropriately tuned to avoid breaking of the chemical bonds in ZnGlyGlyH or ZnGlyGlyPh solely for the 30-min irradiation, which was confirmed by the IR spectra (1651 and 1626 cm^{-1} for ZnGlyGlyH and ZnGlyGlyPh, respectively [19]) prior to other experiments using Lyz. Comparing the IR spectra before and after irradiation, changes in each structure (α-helix and so on) were quantified, and protein secondary structure analysis was performed using IR data with the analytical software, IR-SSE (Jasco Co. Japan) [29].

3. RESULTS AND DISCUSSION

3.1. Damage of Hybrid Materials by IR-FEL Irradiation

First, protein damage by IR-FEL was confirmed using Lyz and two Zn(II) complexes. A previous study confirmed that the most prominent IR bands at 1651 and 1626 cm^{-1} could be assigned to C=N (imine) bonds for ZnGlyGlyH and ZnGlyGlyPh, respectively [16]. In addition to the coordination geometries, no characteristic features of ZnGlyGlyH and ZnGlyGlyPh were found when compared with an analogous Cu(II) complex [21]. Moreover, the IR spectra of Lyz have been reported from several viewpoints, and reliable assignments and discussions have been established [30]. Therefore, the IR-FEL irradiation wavelengths (wavenumbers) were determined to be 1651, 1634, and 1535 cm^{-1} for the imine C=N of the Zn(II) complexes and amide I and II bands of Lyz, respectively. When a beam of relatively low power was used for 30 min, the Zn(II) complexes could not be decomposed [19]. These conditions were used again for control experiments according to a previously reported procedure [19]. Methanol solutions of only Lyz, Lyz-ZnGlyGlyH, and Lyz-ZnGlyGlyPh hybrids were dropped onto a stainless plate and dried to obtain cast films, which were used as samples for IR-FEL irradiation (1651 cm^{-1}) for up to 30 min. The position of the irradiation beam was marked and obtained using an infrared microscope. Among the three samples, under these experimental conditions, significant changes in the IR spectra were exhibited by Lyz-ZnGlyGlyPh, whereas native Lyz did not exhibit any significant change.

As the Lyz films were prepared by casting, keeping the thickness of the sample constant was impossible. In such cases, qualitative data processing cannot be directly performed. However, a comparison of the intensities of the IR spectra for each sample may be reliable because the same sample was analyzed before and after irradiation. For this reason, the abundance ratios of α-helices and β-sheets were compared, which is the established method for analyzing the ratio of secondary structures (Figure 1). Because we did not know where the secondary structure would be cut, we assumed that a change in timing would cause damage. Therefore, data obtained from curve analyses and not statistics for repeated measurements were considered.

No peaks were observed at all wavelengths for the Lyz sample under IR-FEL irradiation, suggesting a marginal effect on secondary structures. In contrast, in the cases of Lyz-ZnGlyGlyH and Lyz-ZnGlyGlyPh, IR-FEL irradiation resulted in

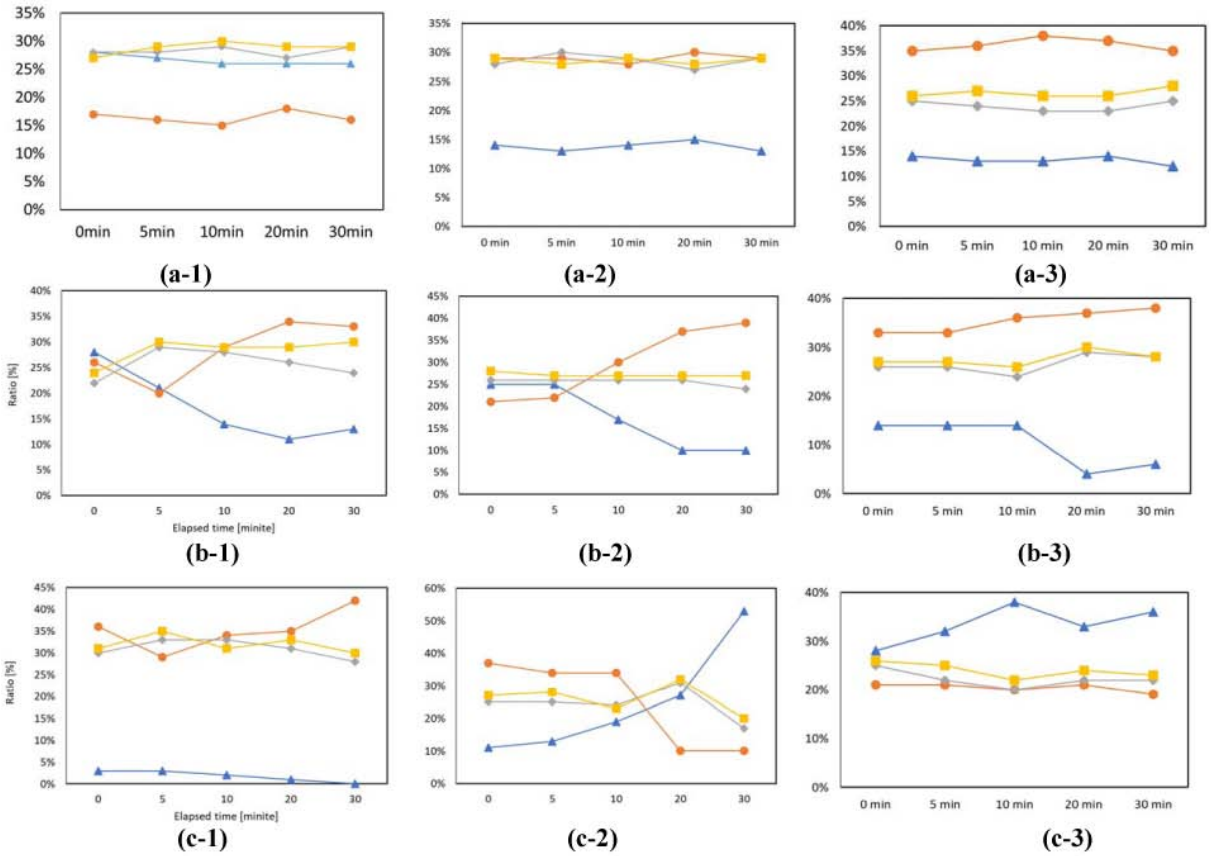

Figure 1. Irradiation-time-dependent protein secondary structure analyses of (a) Lyz, (b) Lyz-ZnGlyGlyH and (c) Lyz-ZnGlyGlyPh irradiated at (1) 1634, (2) 1647, and (3) 1535 cm^{-1} in terms of the α-helix (blue), β-sheet (orange), β-turn (gray), and other (yellow).

relatively significant changes in the secondary structures; in particular, the change in the abundance ratio of the α-helix and β-sheet was remarkable relative to those in the raw spectra. Similar results were observed for HSA and HSA-ZnGlyGlyH or HSA-ZnGlyGlyPh [19]. A high irradiation time caused the ratios of α-helices to increase and those of β-sheets to decrease for HSA-ZnGlyGlyPh. This may be because the introduction of ZnGlyGlyH or ZnGlyGlyPh into Lyz causes secondary structural changes, such as the spiral structure of the α-helix of Lyz unraveling like a β-sheet or the β-sheet swirling in a spiral.

Similarly, not only for the previous HSA [19] but also for the present Lyz, when the hybrid of the Lyz-Zn(II) complex was irradiated with IR-FEL, the secondary structure was disturbed more effectively than the native Lyz (protein only). Based on this finding, the mechanism of structural change should be elucidated by pursuing the docking state at the time of complexing of the Lyz and Zn(II) complex by optical measurement. However, solid film samples are unsuitable for circular dichroism (CD) spectroscopy measurements.

3.2. Fluorescence spectra

Herein, weak, non-steady, and non-covalent bonding interactions between protein molecules and the two Zn(II) complexes are discussed using several measurements of fluorescence spectroscopy, in addition to CD spectroscopy. To reveal the effect of the additional Zn(II) complexes and determine the docking features and behavior of the Zn(II) complexes and Lyz, several types of fluorescence spectroscopy (Förster resonance energy transfer (FRET) [31], quenching [32], temperature dependence [33], and lifetime [34]) measurements were

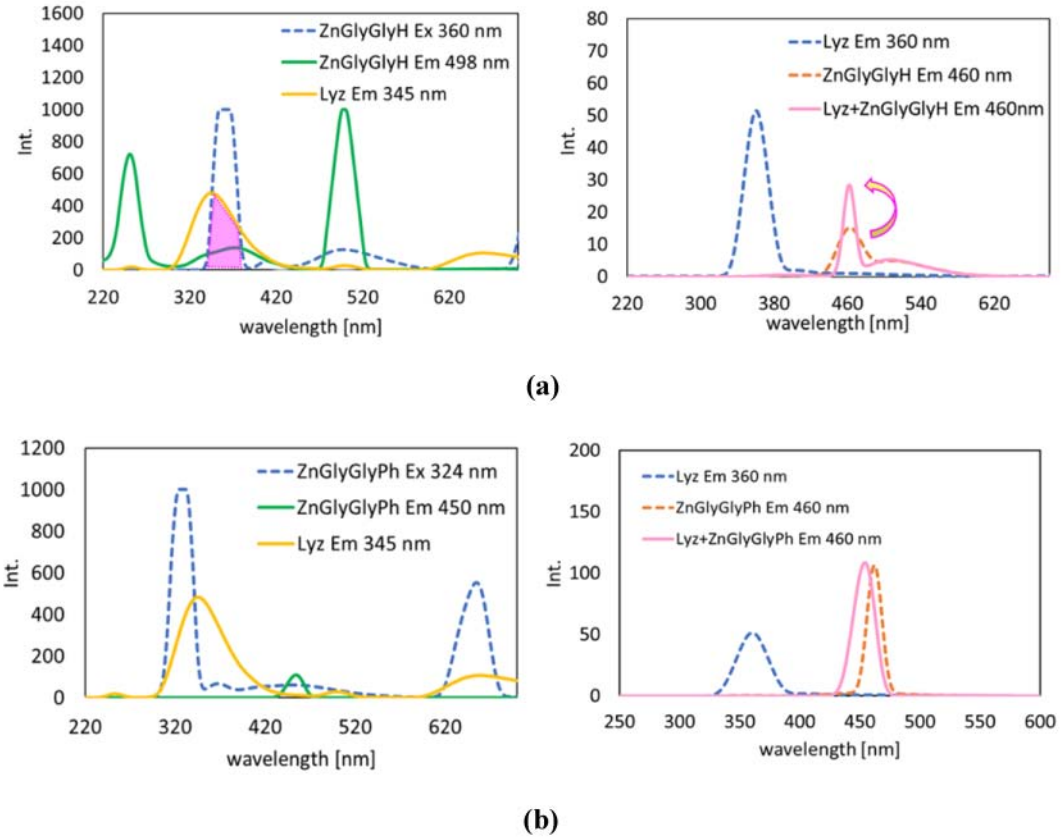

Figure 2. Fluorescence spectra of (a) Lyz-ZnGlyGlyH and (b) Lyz-ZnGlyGlyPh with the explanation of FRET *via* intermolecular short contact.

conducted. A1:1 (v/v) solution of the Zn(II) complex (0.5 mM in methanol) and Lyz (0.5 mM in a phosphate buffer) was used. The concentration of the solution was gradually increased.

According to a previous study [19] and the corresponding 3D spectra, the ZnGlyGlyH excitation wavelengths were 360 and 240 nm; emission wavelengths were 454 and 458 nm; ZnGlyGlyPh excitation wavelengths were 380, 320, and 260 nm; emission wavelengths were 451 and 449 nm; Lyz excitation wavelengths were 570 and 280 nm; and emission wavelengths were 667, 349, and 352 nm (Figure 2).

According to the emission wavelength (345 nm) of lysozyme, we confirmed it to be the donor. According to the excitation wavelength (360 nm) of the Zn(II) complex, we confirmed it to be the acceptor. Under these conditions, the fluorescence intensity at 460 nm, which is the emission wavelength of ZnGlyGlyH, was approximately twice that of a single substance; however, there was no change in ZnGlyGlyPh (Figure 2).

When the emission wavelength of the substance that becomes the donor and the excitation wavelength of the substance that becomes the acceptor are similar, the emission intensity of the acceptor becomes higher than that of a single substance. Furthermore, this reaction occurs only *via* a dynamic quenching mechanism, as energy transfer occurs when the donor is in an excited state. The distance between the donor and acceptor must be reasonably small (≤10 nm) to cause energy transfer. Because the donor is Lyz and the acceptor is the Zn(II) complex, we measured the emission intensity at 460 nm, which is the emission wavelength of the Zn(II) complex.

Fluorescence lifetime measurement based on TCSPC was conducted (Figure 3), and two-dimensional data of “time (life)” and “number of photons at each time” were acquired. This measurement provides

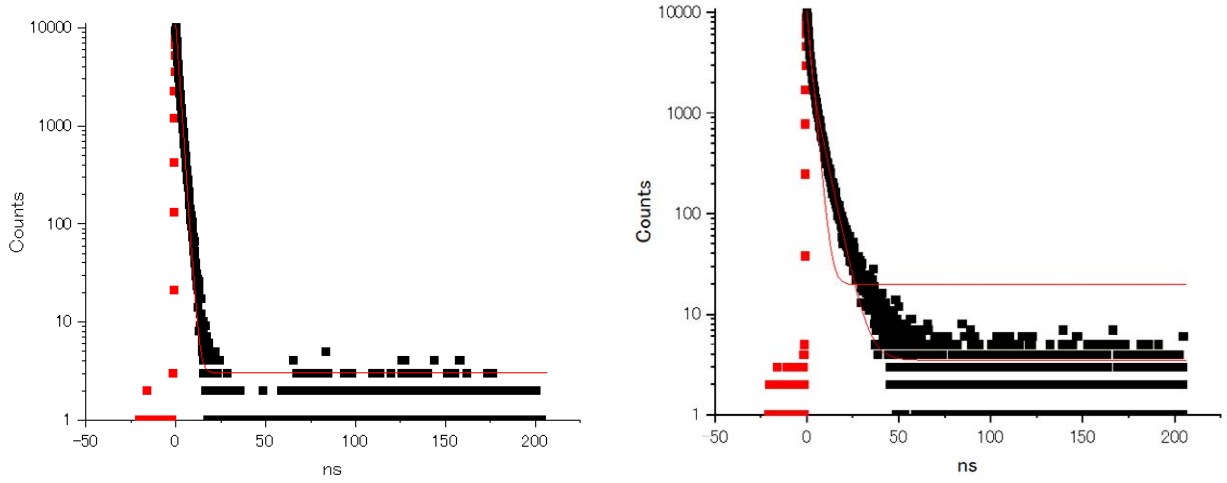

(a) **(b)**

Figure 3. Fluorescence lifetime measurements for (a) Lyz-ZnGlyGlyH fitted to $y = A_1\exp(-x/t_1)$ with $y_0 = 3.0047 \pm 1.6156$, $A_1 = 10984.62$, $t_1 = 1.6264 \pm 0.0073$, and $R = 0.99071$ and (b) Lyz-ZnGlyGlyPh fitted to $y_0 = A_1\exp(-x/t1) + A_2\exp(-x/t_2)$ with $y_0 = 3.52827 \pm 1.0342$, $A_1 = 7579.152 \pm 67.718$, $t_1 = 1.15944 \pm 0.01409$, $A_2 = 3154.625 \pm 72.313$, $t_2 = 4.94495 \pm 0.0735$, and $R = 0.9966$. The red lines of different fitting functions indicate the different curvatures of dots. This is not a repeated measurement or statistic.

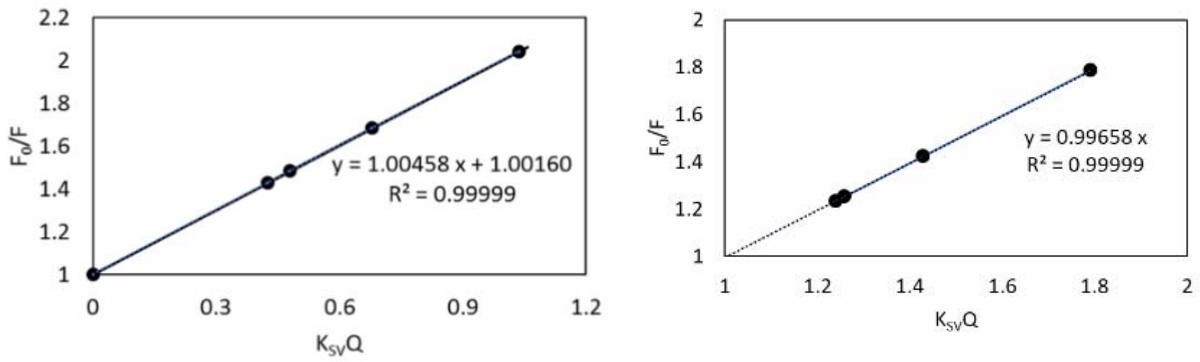

(a) **(b)**

$$\frac{F_0}{F} = 1+K_{sv}[Q]=1+k_q t_0[Q]$$

F_0:Fluorescence intensity in the absence of quencher
F: Fluorescence intensity in the presence of quencher
K_{sv}: Quenching constant
t_0: Fluorescence lifetime (1.87 ns for lysozyme)
k_q: Two-molecule quenching rate constant
[Q]:Solution concentration (0.5 mM)

Figure 4. Stern–Volmer plots of the reduction in fluorescence intensity with regression lines for (a) Lyz-ZnGlyGlyH and (b) Lyz-ZnGlyGlyPh (Above). Stern–Volmer equation with parameters (Below).

information regarding the number of luminescent species and the radiative and nonradiative rate constants in the sample. By obtaining the number of luminescent species, we could confirm whether it was bound to Lyz or existed in an equilibrium state. Simultaneously, we measured the fluorescence lifetimes of Lyz-ZnGlyGlyH and Lyz-ZnGlyGlyPh at 470 nm and assigned a function from the decay curve fitting. Results indicated that Lyz-ZnGlyGlyH exhibited single exponential decay, whereas Lyz-ZnGlyGlyPh exhibited double exponential decay. As Lyz-ZnGlyGlyH displayed only one luminescent species, it is suggested that Lyz and ZnGlyGlyH may be bound and exist as one luminescent species. Lyz and ZnGlyGlyPh may also be bound but have another decay path, which might be related to a different fluorescence quenching behavior, as shown in Figure 4.

Overlapping graphs with FRET were confirmed for both complexes. As ZnGlyGlyH was detected when the emission intensity at 460 nm doubled, FRET occurred, which could be interpreted as dynamic quenching [35] obtained from the data of decreasing intensity using the Stern–Volmer relationship (Figure 4). In contrast, with ZnGlyGlyPh, there was no change in the fluorescence intensity at 460 nm. FRET did not occur, and static quenching was confirmed [36]. Furthermore, a decrease in fluorescence intensity was observed for the complexes of ZnGlyGlyH, ZnGlyGlyPh, and Lyz. Typically, the higher the concentration of fluorescent molecules, the lower the fluorescence intensity. Furthermore, when fluorescent molecules are mixed, the fluorescence intensity decreases because of the interaction between the fluorescent molecules. Both complexes were quenched, indicating the docking of the Lyz and Zn(II) complexes. Two types of interactions—excited and ground states—were observed.

Fluorescence measurements indicated that the interaction between the two molecules extinguished the light. Therefore, the quenching mechanism was investigated. Quenching is classified into two types: dynamic, which occurs owing to energy transfer when the donor is in the excited state, and static, which occurs when the donor and acceptor molecules are in the ground state. To distinguish this, the diatomic quenching rate constant (k_q) was calculated from the fluorescence intensity at different temperatures. In general, these data resulted from the quenching mechanism. At higher temperatures, the k_q of ZnGlyGlyPh increased, while the k_q of ZnGlyGlyH decreased (Table 1), suggesting different features of intermolecular interactions against Lyz for ZnGlyGlyH and ZnGlyGlyPh.

3.3. Molecular docking features

As direct observation of the docking of protein and Zn(II) complexes is experimentally impossible, computational simulation of molecular docking was conducted to corroborate the intermolecular interaction suggested by the spectroscopic results. Results of computational docking simulation showed that the Zn(II) complexes (namely, Lyz - ZnGlyGlyH and Lyz-ZnGlyGlyPh) were docked with the highest scores (evaluated by a GOLD program) of 41.51 and 37.74, respectively (Figure 5). Both non-covalent docking sites showed high

Table 1. Temperature dependence of the K_{SV} and k_q parameters of the Stern–Volmer equation.

	T(K)	K_{SV} (10^4 M^{-1})	k_q (10^{13} $M^{-1}s^{-1}$)
Lyz-ZnGlyGlyH	298	2.072	1.108
	293	1.357	0.726
	297	0.959	0.513
	311	0.852	0.455
Lyz-ZnGlyGlyPh	298	2.048	1.095
	293	2.342	1.253
	297	3.045	1.628
	311	4.306	2.302

values for the structurally open space of lysozyme [37, 38]. The non-covalent distances were shortest, with ZnGlyGlyH at tryptophan 108 and 4.631 Å and ZnGlyGlyPh at tryptophan 63 and 1.935 Å. Potentially, three types of ligand-binding sites exist for proteins, although their computational prediction may sometimes be difficult [39]. The first is an active bond, in which the ligand binds to an amino acid residue with a non-covalent pair in the protein, while the second is an active bond, in which the amino acid residue is coordinated at multiple positions. The third is an inactive bond that coexists at equilibrium without a binding site. In general, coordination of Zn(II) complexes to the nitrogen atom of histidine residues [40] may not be easier than that of Cu(II) complexes [41] in a cold buffer solution. Therefore, we considered non-covalent docking features for computation, which is supported by the following experimental results.

A saturated aqueous solution of the Zn(II) complex was added to a single crystal of Lyz to prepare a Zn(II) complex-containing crystals. By observing the electron density, determining the binding or equilibrium of metal ions or complexes is possible [42]. Immersion of the Zn(II) complex in the lysozyme crystal was confirmed by the change in crystal color. Pale yellow is the color of the imine group of the Schiff-base Zn(II) complex, although Zn(II) ions cannot exhibit visible color due to the *d–d* transition [43]. The crystals of Lyz were almost colorless and transparent [44] but turned yellow when immersed in the complex.

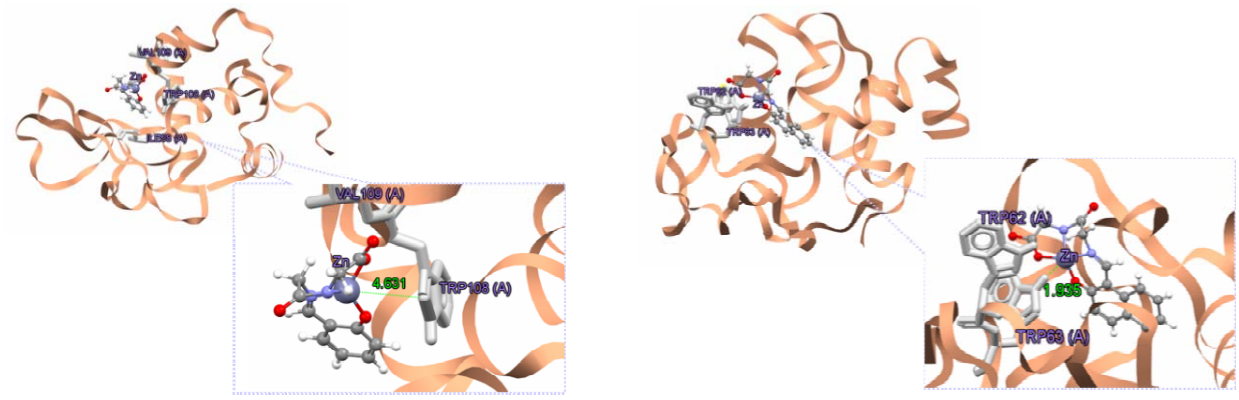

Figure 5. Docking simulation of (a) Lyz-ZnGlyGlyH and (b) Lyz-ZnGlyGlyPh using a GOLD program based on crystal structures.

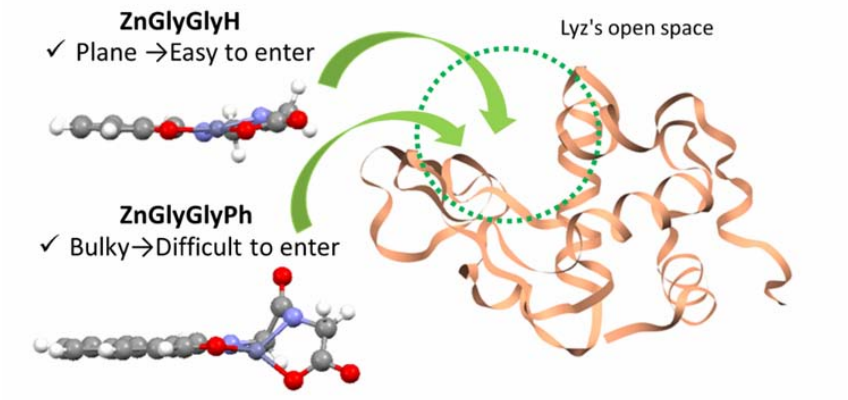

Figure 6. Difference in the molecular docking features of the two Zn(II) complexes.

Because ZnGlyGlyH has a planar structure and ZnGlyGlyPh has a distorted and bulky structure, the difference may be attributed to the difficulty of entering the gap of the molecular surface of Lyz. Results of the docking simulation is likely to be present in the Lyz gap. To enter the gap, planar structures such as ZnGlyGlyH exhibited less damage, could enter deeper, and had a stronger interaction with Lyz. In contrast, the bulky structure of ZnGlyGlyPh was a major obstacle to invasion, weakening its interaction with Lyz and causing this difference (Figure 6).

4. CONCLUSION

In a previous study, we assumed that a dipeptide complex would absorb IR light corresponding to amide bands to protect proteins from IR-FEL irradiation, although damage to proteins was enhanced by a dipeptide complex. In this work, we indicated the effect of adding a metal complex for protection from damage against IR-FEL irradiation and examined it using different complexes or proteins. We confirmed this effect by applying another protein (chicken egg white lysozyme, a well-known and basic protein) in addition to HSA for the first time using the same complexes.

The results of docking simulation indicated that the metal complex was likely to dock with lysozyme. Quenching measurements revealed that the two molecules were close together and were likely to be docked because quenching occurred when Lyz and Zn(II) complexes were combined. Furthermore, ZnGlyGlyH generated FRET, whereas ZnGlyGlyPh did not. Results indicated that the quenching mechanism depends on the complex; therefore, we measured the fluorescence lifetime and attempted to clarify the docking state from the number of luminescent species of the Lyz-Zn(II) complex to Lyz. As a result, ZnGlyGlyH had one emitting species, while ZnGlyGlyPh had two luminescent species. Thus, it is considered that ZnGlyGlyH is directly bound to Lyz, one luminescent species is generated, and ZnGlyGlyPh coexists in an equilibrium state, resulting in two types. To confirm the binding to ZnGlyGlyH and determine whether it was actually docked at that location, we conducted single-crystal electron density analysis. As a result, only (native) lysozyme was obtained, and the Zn(II) complex was not observed. The two molecules were found to be docked; however, they were not directly bonded and were likely to coexist in an equilibrium state or interact with a weak bond such as a hydrogen bond.

For the realization of practical applications, challenges exist in satisfying various purposes and opinions. The following opinions exist regarding research proposals that complemented simulation calculations and experiments for COVID-19. For example, experiments are apparently only possible if individual proteins are used. Disinfectants such as alcohol are often used for hand washing and wiping to remove viral proteins. In contrast, there are some uses, such as those concerning food, that are not suitable for drugs, and the decomposition of virus molecules by light is worth investigating. In reality, it is impossible to assume the use of the current infrared free-electron laser for sterilization and medical use in social life. For the practical use of IR-FEL, it must be inexpensive and have widespread access. Currently, this technology is limited to a basic research or testing level.

ACKNOWLEDGMENTS

This work was partly supported by a Grant-in-Aid for Scientific Research (A) KAKENHI (20H00336).

CONFLICT OF INTEREST STATEMENT

There are no conflicts to declare.

ABBREVIATIONS

FELs, Free-electron lasers; IR-FEL, Infrared free-electron laser; DFT, density functional theory; NPSs, novel psychotropic drugs; HSA, human serum albumin; IL-6, Interleukin-6; PBS, phosphate-buffered saline; TCSPC, Time-correlated single-photon counting; PXRD, Powder X-ray diffraction; PCM, polarizable continuum model; CD, circular dichroism; FRET, Förster resonance energy transfer.

REFERENCES

1. O'Shea, P. G. and Freund, H. P. 2001, Science, 292, 1853.
2. Kim, K.-J. and Sessler, A. 1990, Science, 250, 88.
3. Murdin, B. N. 2009, Contemporary Phys., 50, 391.

4. Austin, R. H., Xie, A., van der Meer, L., Redlich, B., Lindgård, P.-A., Frauenfelder H. and Fu, D. 2005, Phys. Rev. Lett., 94, 128101.
5. Bouchet, A., Klyne, J., Ishiuchi, S.-i., Fujii, M. and Dopfer, O. 2017, Phys. Chem. Chem. Phys., 19, 10767.
6. Kranenburg, R. F., van Geenen, F. A. M. G., Berden, G., Oomens, J., Martens, J. and van Asten, A. C. 2020, Anal. Chem., 92, 7282.
7. Wilmink, G. J., Opalenik, S. R., Beckham, J. T., Mackanos, M. A., Nanney, L. B., Contag, C. H., Davidson, J. M. and Jansen, E. D. 2008, J. Biomedical Optics, 13, 054066.
8. Sakamoto, F. H., Doukas, A. G., Farinelli, W. A., Tannous, Z., Shinn, M., Benson, S., Williams, G. P., Gubeli III, J. F., Dylla, H. F. and Anderson, R. R. 2012, Lasers in Surgery and Medicine, 44, 175.
9. Fraschetti, C., Filippi, A., Guarcini, L., Steinmetz, V. and Speranza, M. 2015, J. Phys. Chem. B, 119, 6198.
10. Lacerda, S., Morfin, J.-F., Geraldes, C. F. G. C. and Tóth, É. 2017, Dalton Trans., 46, 14461.
11. Wärmländer, S., Tiiman, A., Abelein, A., Luo, J., Jarvet, J., Söderberg, K. L., Danielsson, J. and Gräslund, A. 2013, ChemBioChem, 14, 1692.
12. Parthasarathy, S., Long, F., Miller, Y., Xiao, Y., McElheny, D., Thurber, K., Ma, B., Nussinov, R. and Ishii, Y. 2011, J. Am. Chem. Soc., 133, 3390.
13. Kinebuchi, M., Matsuura, A., Kiyono, T., Nomura, Y. and Kimura, S. 2016, Sci. Rep., 6, 33247.
14. Grasso, G. and Bonnet, S. 2014, Metallomics, 6, 1346.
15. Kawasaki, T., Tsukiyama, K. and Irizawa, A. 2019, Sci. Rep., 9, 10636.
16. Kawasaki, T., Yaji, T., Ohta, T., Tsukiyama, K. and Nakamura, K. 2018, Cell. Mol. Neurobio., 38, 1039.
17. Kawasaki, T., Fujioka, J., Imai, T. and Tsukiyama, K. 2012, Protein J., 31, 710.
18. Onami, Y., Kawasaki, T., Aizawa, H., Haraguchi, T., Akitsu, T., Tsukiyama, K. and Palafox, M. A. 2020, Int. J. Mol. Sci., 21, 874.
19. Onami, Y., Koya, R., Kawasaki, T., Aizawa, Nakagame, R., Miyagawa, Y., H.; Haraguchi, T., Akitsu, T., Tsukiyama, K. and Palafox, M. 2019, Int. J. Mol. Sci., 20, 2846.
20. Fujisawa, N., Onami, Y., Kawasaki, T., Haraguchi, T., Akitsu, T. and Tsukiyama, K. 2020, Trends in Peptide and Protein Sciences, 5, e8.
21. Kashiwagi, K., Tassinari, F., Haraguchi, T., Banerjee-Gosh, K., Akitsu, T. and Naaman, R. 2020, Symmetry, 12, 808.
22. Zhoug, Y. and Patel, S. 2013, J. Comput. Chem., 34, 163.
23. Available online: https://www.ccdc.cam.ac.uk/solutions/csd-discovery/Components/Gold/ (accessed on 2020.7.27).
24. Schmidt, M. W., Baldridge, K. K., Boatz, J. A., Elbert, S. T., Gordon, M. S., Jensen, J. H., Koseki, S., Matsunaga, N., Nguyen, K. A. and Su, S. 1993, J. Comput. Chem., 14, 1347.
25. Gordon, M. S. and Schmidt, M. W. 2005, Advances in Electronic Structure Theory, Elsevier, Amsterdam.
26. Tawada, Y., Tsuneda, T., Yanagisawa, S., Yanai, T. and Hirao, K. 2004, J. Chem. Phys., 120, 8425.
27. Kawasaki, T., Yaji, T., Ohta, T. and Tsukiyama, K. 2016, J. Synchrotron Rad., 23, 152.
28. Yokoyama, M., Oda, F., Nomaru, K., Koike, H., Sobajima, M., Miura, H., Hattori, H., Kawai, M. and Kuroda, H. 2001, Nucl. Instrum. Methods Phys. Res., 475, 38.
29. Sarver, R. W. Jr. and Krueger, W. C. 1991, Anal. Biochem., 194, 89.
30. Islam, Z., Ali, M. H., Popelka, A., Mall, R., Ullah, E., Ponraj, J. and Kolatkar, P. R. 2021, J. Biomol. Struct. Dynamics, 39, 1481.
31. Trusova, V. M., Gorbenko, G. P., Sarkar, P., Luchowski, R., Akopova, I., Patsenker, L. D.,Klochko, O., Tatarets, A. L., Kudriavtseva, Y. O., Terpetschnig, E. A., Gryczynski, I. and Gryczynski, Z. 2010, J. Phys. Chem. B, 114, 16773.
32. Han, G., Feng, N. and Wang, G. 2014, Chem. Lett., 43, 1499.
33. Ding, F., Zhao, G., Huang, J., Sun, Y. and Zhang, L. 2009, Eur. J. Med. Chem., 44, 4083.

34. Yamashita, S., Nishimoto, E. and Yamasaki, N. 1995, Biosci. Biotech. Biochem., 59, 1255.
35. Butkus J. M., O'Riley, S., Chohan, B. S. and Basu, S. 2016, Int. J. Spectr., 1.
36. McGruire, R. and Feldman, I. 1975, Biopolymers, 14, 1095.
37. Ioue, M., Yamada, H., Yasukochi, T., Kuroki, R., Miki, T., Horiuchi, T. and Imoto, T. 1992, Biochem. 31, 5545.
38. Teshima, K., Kuramitsu, S., Hamaguchi, K., Sakiyama, F. and Yamasaki, N. 1980, J. Biochem., 87, 1015.
39. Sciortino, G., Garribba, E. and Maréchal, J.-D. 2019, Inorg. Chem., 58, 294.
40. Zhou, L., Li, S., Su, Y., Yi, X., Zheng, A. and Deng, F. 2013, J. Phys. Chem. B, 117, 8954.
41. Thompsett, A. R., Abdelraheim, S. R., Daniels, M. and Brown, D. R. 2005, J. Bio. Chem., 280, 4270.
42. Mizutani, R., Shimizu, Y., Saiga, R., Ueno, G., Nakamura, Y., Takeuchi, A., Uesugi, K. and Suzuki, Y. 2014, Sci. Rep., 4, 5131.
43. Akitsu, T. and Itoh, T. 2010, Polyhedron, 29, 477.
44. Yan, E.-K., Lu, Q.-Q., Zhang, C.-Y., Liu, Y.-L., He, J., Chen, D., Wang, B., Zhou, R.-B., Wu, P. and Yin, D. C. 2016, Sci. Rep., 6, 34770.